Modeling plane turbulent Couette flow*

H. I. Andersson and B. A. Pettersson
Department of Applied Mechanics, Thermodynamics and Fluid Dynamics, The Norwegian Institute of Technology, Trondheim, Norway

Among the salient features of shear-driven plane Couette flow is the constancy of the total shear stress (viscous and turbulent) across the flow. This constancy gives rise to a quasi-homogeneous core region, which makes the bulk of the flow substantially different from pressure-driven Poiseuille flow. The present second-moment closure study addresses the conflicting hypotheses relating to turbulent Couette flow. The inclusion of a new wall-proximity function in the wall-reflection part of the pressure-strain model seems mandatory, and the agreement with recent experimental and direct numerical simulation (DNS) results is encouraging. Analysis of model computations in the range $750 \leq \mathrm{Re} \leq 35{,}000$ and comparisons with low-Re DNS data suggest that plane Couette flow exhibits a local-equilibrium core region, in which anisotropic, homogeneous turbulence prevails. However, the associated variation of the mean velocity in the core, as obtained by the model, conflicts with the intuitively appealing assumption of homogeneous mean shear. The constancy of the velocity gradient exhibited by the DNS therefore signals a deficiency in the modeled transport equation for the energy dissipation rate.

Keywords: turbulence; channel flow; second-moment modeling; near-wall closures

1. Introduction

The plane Couette flow is the shear-driven motion of fluid bounded by two parallel planes in relative motion. The Couette flow is turbulent in the majority of practical cases, e.g., engineering flows associated with lubrication technology, thin-film coating, and stratified two-phase flow, and in natural flows like the wind-induced motion in shallow lakes. From a turbulence modeler's point of view, the conceptually simple *fully developed* turbulent Couette flow between two infinite plates is particularly attractive due to its homogeneity in planes parallel with the bounding plates. Among its outstanding features are the unidirectional fluid motion and the constancy of the shear stress across the flow. Moreover, within the framework of turbulent transport modeling, any set of differential model equations reduces to a set of ordinary differential equations in the coordinate y perpendicular to the plates.

The possible existence of a constant mean shear rate dU/dy in the core region of turbulent Couette flow led von Kármán (1937) to introduce the concept of *homologous* turbulence. Robertson and Johnson (1970) pointed out that the rate of turbulence energy production is constant in the homologous or quasi-homogeneous core region, and they moreover conjectured that the production and dissipation of mean turbulent kinetic energy must balance at every point in this region. In contrast, Schneider (1989) proposed a new turbulence model that allows for significant countergradient diffusion of turbulent energy from the core towards the walls. By adding to the standard gradient-diffusion model a diffusive term that takes variation of an integral length scale into account, Schneider obtained surprisingly good agreement with the remarkable low energy level measured in the Couette flow apparatus of El Telbany and Reynolds (1980, 1981, 1982). Gibson (1988) demonstrated that with Schneider's new diffusion model only half of the turbulent energy in the core is dissipated locally, while the other half is diffused away from the center.

Attempts to compute the plane Couette flow with a k–ε model (Henry and Reynolds 1984) and Reynolds stress closures (Schneider 1989; Obi et al. 1989) led to a uniform level of turbulent kinetic energy across the flow and an associated balance between energy production and dissipation. A common feature of these studies is the application of the wall-function approach in order to match the numerical solution to some local-equilibrium conditions at the wall-adjacent node. Nisizima and Yoshizawa (1987), however, adopted an anisotropic k–ε closure and solved the model equations directly into the walls. Nevertheless, they failed to reproduce the experimentally observed near-wall peaks. Monnier and Stanislas (1989) considered three of the available low-Reynolds-number extensions of the high-Re k–ε model. Two of these models predicted a local energy maximum near the walls, but the energy level in the core region was appreciably higher than in the extensive experiments by El Telbany and Reynolds (1980, 1981, 1982).

Very recently, three independent attempts to model the plane Couette flow led to inconclusive results. Zhang et al. (1993) used a low-Re extension of a standard second-moment closure and arrived at the puzzling conclusion that their prediction was actually worse than that of a k–ε model. Sund (1993) and Andersson et al. (1993) adopted the second-moment near-wall closure of Launder and Shima (1989) and obtained reasonable results after having introduced brute-force modifications in the original model. More specifically, a wall-damping function that accounted for only one wall at a time was introduced by Sund (1993), while the originally isotropic model for the dissipation rate tensor was replaced by an anisotropic model by Andersson et al. (1993) in order to achieve numerical convergence.

In spite of its conceptual simplicity, fully developed Couette flow is rather difficult to realize in the laboratory; see, e.g.,

---

* This article is a revised version of Paper 94-2342 presented at the 25th AIAA Fluid Dynamics Conference, June 20–23, 1994, in Colorado Springs, CO, USA

Address reprint requests to Professor Andersson at the Department of Applied Mechanics, Thermodynamics and Fluid Dynamics, The Norwegian Institute of Technology, N-7034 Trondheim, Norway.

Received 15 April 1994; accepted 23 July 1994

Aydin and Leutheusser (1987, 1991). Fully developed flows are, on the other hand, particularly attractive objects for direct numerical simulations (DNSs). The recently undertaken DNSs (e.g., Lee and Kim 1991; Kristoffersen et al. 1993) of plane Couette flow provide valuable guidance for a better understanding and more reliable modeling of this particular flow field. Guided by our in-house DNS data (Kristoffersen et al. 1993) and supplemented by the most recent laboratory experiments (Tillmark and Alfredsson 1993) of fully developed Couette flow, the purpose of the present investigation is to address the conflicting hypotheses relating to this flow, thereby attempting to resolve the apparent difficulties associated with the modeling of the seemingly simple flow.

2. Physical model problem

The problem considered is that of steady turbulent Couette flow between two infinite parallel planes, as shown schematically in Figure 1. This constant-pressure flow is induced solely by the relative motion of the two planes, of which the lower is at rest and the upper is moving at a constant velocity U_w in the positive x-direction. The Reynolds-averaged Navier–Stokes equation governing the transport of streamwise mean momentum can be written as

$$0 = \frac{d}{dy}\left(\mu \frac{dU}{dy} - \rho\overline{uv}\right) \tag{1}$$

for a constant property fluid. Since the mean velocity vector $\mathbf{V} = (U(y), 0, 0)$ is aligned with the planes, the continuity constraint $\partial U_i/\partial x_i = 0$ is automatically satisfied. The a priori unknown Reynolds shear stress, $-\rho\overline{uv}$, in Equation 1 can be obtained from the transport equation

$$\frac{D\overline{u_i u_j}}{Dt} = P_{ij} - \varepsilon_{ij} + \phi_{ij} + D_{ij} + \nu \frac{d^2\overline{u_i u_j}}{dy^2} \tag{2}$$

for the second-moments $\overline{u_i u_j}$. The rate of stress production due to mean shear,

$$P_{ij} = -\left[\overline{u_i u_k}\frac{\partial U_j}{\partial x_k} + \overline{u_j u_k}\frac{\partial U_i}{\partial x_k}\right] \tag{3}$$

involves only mean velocity gradients and the Reynolds stresses themselves, whereas the rates of viscous dissipation ε_{ij}, pressure-strain interactions ϕ_{ij}, and turbulent diffusion D_{ij} require extensive modeling. Since the steady flow under consideration is homogeneous in the (xz)-planes, the rate-of-change $D\overline{u_i u_j}/Dt = 0$, and the only nonzero production terms are $P_{11} = -2\overline{uv}\, dU/dy$ and $P_{12} = P_{21} = -\overline{v^2}\, dU/dy$.

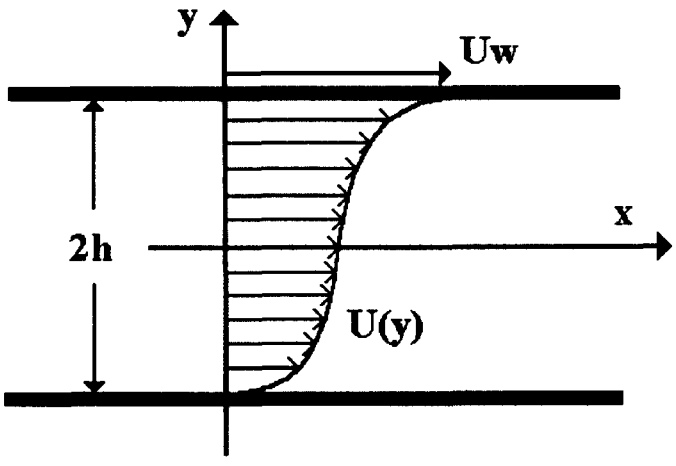

Figure 1 Schematic of plane turbulent Couette flow

3. Turbulence modeling

3.1. Reynolds stress transport model

The widely used second-moment closure for near-wall turbulence proposed by Launder and Shima (1989) has been adopted in the present study. This model has been applied to a number of boundary-layer problems (Launder and Shima 1989; Shima 1993a, 1993b) and was among the eight near-wall Reynolds-stress closures scrutinized by So et al. (1991). In spite of an incorrect asymptotic behavior at the wall, the overall performance is quite convincing. Here, we are not concerned about the flow in the immediate vicinity of the planes, and the Launder and Shima model should therefore be an appropriate choice.

The Launder and Shima model is essentially an extension of a well-established high-Reynolds-number model (Gibson and Launder 1978) intended to account for the wall effects in the viscous sublayer. First, the turbulent stress diffusion associated

Notation

a_{ij}	Reynolds stress anisotropy, $\overline{u_i u_j}/k - 2\delta_{ij}/3$
A	Anisotropy parameter, $1 - 9(A_2 - A_3)/8$
A_2	Second invariant, $a_{ij}a_{ij}$
A_3	Third invariant, $a_{ik}a_{kj}a_{ji}$
A_{max}	Maximum value of A
C_f	Skin-friction coefficient, $2(\tau_w/\rho)/(U_w/2)^2$
d	Effective wall distance
D_{ij}	Turbulent diffusion of Reynolds stresses
f	Wall-proximity function
f^{new}	New wall-proximity function
g	Weighting function, $(1 - A/A_{max})^2$
h	Channel half-width
k	Turbulent kinetic energy, $\overline{u_i u_i}/2$
P	Generation rate of kinetic energy, $P_{ii}/2$
P_{ij}	Shear generation rate of $\overline{u_i u_j}$
Re_t	Turbulent Reynolds number, $k^2/\nu\varepsilon$
Re	Reynolds number, hU_w/ν
u, v	Velocity fluctuations in x- and y-directions
$u_{i,rms}$	Turbulence intensity in x_i-direction
$\overline{u_i u_j}$	Kinematic Reynolds stress
u_τ	Wall friction velocity, $(\tau_w/\rho)^{1/2}$
U_w	Wall speed
x_i	Cartesian coordinate
x, y	Coordinates defined in Figure 1
y^+	Inner variable, $(h + y)u_\tau/\nu$

Greek symbols

ε	Energy dissipation rate, $\varepsilon_{ii}/2$
ε_{ij}	Dissipation rate tensor
μ	Dynamic viscosity
ν	Kinematic viscosity, μ/ρ
ρ	Density
τ	Total shear stress, $\mu dU/dy - \rho\overline{uv}$
τ_w	Wall shear stress
ϕ_{ij}	Pressure-strain interactions

with velocity and pressure fluctuations is represented by the generalized-gradient-diffusion hypothesis

$$D_{ij} = \frac{d}{dy}\left[C_s \frac{k}{\varepsilon}\overline{v^2}\frac{\overline{du_i u_j}}{dy}\right] \tag{4}$$

whereas the dissipation rate tensor ε_{ij} is assumed to be locally isotropic, i.e.,

$$\varepsilon_{ij} = \frac{2}{3}\delta_{ij}\varepsilon \tag{5}$$

The pressure-strain correlation tensor ϕ_{ij} is conventionally split into four different parts, $\phi_{ij,1} + \phi_{ij,2} + \phi^w_{ij,1} + \phi^w_{ij,2}$, which are modeled separately as

$$\phi_{ij,1} = -C_1 \frac{\varepsilon}{k}\left(\overline{u_i u_j} - \frac{2}{3}\delta_{ij}k\right) \tag{6}$$

$$\phi_{ij,2} = -C_2\left(P_{ij} - \frac{2}{3}\delta_{ij}P\right) \tag{7}$$

$$\phi^w_{ij,1} = C^w_1 \frac{\varepsilon}{k}\left(\overline{v^2}\delta_{ij} - \frac{3}{2}\overline{vu_i}\delta_{j2} - \frac{3}{2}\overline{vu_j}\delta_{i2}\right)f \tag{8}$$

$$\phi^w_{ij,2} = C^w_2\left(\phi_{22,2}\delta_{ij} - \frac{3}{2}\phi_{2i,2}\delta_{j2} - \frac{3}{2}\phi_{2j,2}\delta_{i2}\right)f \tag{9}$$

where the wall-proximity function f is defined as

$$f = C_d \frac{k^{3/2}/\varepsilon}{d} \tag{10}$$

and the effective wall distance d varies as

$$\frac{1}{d} = \left(\frac{1}{h+y} + \frac{1}{h-y}\right) \tag{11}$$

in order to account for the influence from both walls.

Finally, in order to close the system of model equations, the dissipation rate ε of the turbulent kinetic energy is obtained from its own modeled transport equation

$$\frac{D\varepsilon}{Dt} = \frac{d}{dy}\left[\left(\nu + C_\varepsilon \frac{k}{\varepsilon}\overline{v^2}\right)\frac{d\varepsilon}{dy}\right] + C_{\varepsilon 1}\frac{\varepsilon}{k}P - C_{\varepsilon 2}\frac{\varepsilon\tilde{\varepsilon}}{k} \tag{12}$$

where

$$\tilde{\varepsilon} = \varepsilon - 2\nu\left(\frac{dk^{1/2}}{dy}\right)^2 \tag{13}$$

is negligibly different from ε outside the viscous sublayer. In the problem at hand, the dissipation rate is a function of y only, and the rate-of-change $D\varepsilon/Dt = 0$.

The essence of the Launder and Shima approach is that some of the model coefficients that appear in the high-Reynolds-number closure outlined above are made functions of four dimensionless turbulence characteristics, namely, the turbulent Reynolds number Re_t, the Reynolds stress invariants A_2 and A_3, and the ratio of production to dissipation of turbulent kinetic energy P/ε. Moreover, the local isotropy model (Equation 5) for the dissipation rate tensor is retained, and the expected anisotropy of ε_{ij} in the near-wall region is absorbed in the pressure-strain model.

The recommended low-Re expressions are

$$C_1 = 1 + 2.58AA_2^{1/4}[1 - \exp\{-(0.0067\mathrm{Re}_t)^2\}] \tag{14}$$

$$C_2 = 0.75A^{1/2} \tag{15}$$

$$C^w_1 = -2C_1/3 + 1.67 \tag{16}$$

Table 1 Constants in the Launder–Shima closure

C_s	C_d	C_ε	$C_{\varepsilon 2}$
0.22	0.40	0.18	1.90

$$C^w_2 = \max\left[(2C_2/3 - 1/6)/C_2, 0\right] \tag{17}$$

$$C_{\varepsilon 1} = 1.45 + \psi_1 + \psi_2 \tag{18}$$

with

$$\psi_1 = 2.5A(P/\varepsilon - 1) \tag{19}$$

$$\psi_2 = 0.3(1 - 0.3A_2)\exp\left[-(0.002\mathrm{Re}_t)^2\right] \tag{20}$$

and the remaining coefficients take their standard values as given in Table 1. Shima (1993a, 1993b) recently advocated modified values of the constants in the functions ψ_1 and ψ_2, but the original set of constants are retained in the present study.

3.2. A new model for the near-wall damping function

The wall-correction model $\phi^w_{ij,1} + \phi^w_{ij,2}$ was originally designed for the logarithmic region of a turbulent boundary layer and as such was intended to vanish further away from the wall. In a fully developed channel flow, on the other hand, the role of the wall corrections may prevail into the core of the flow (see, e.g., Abid and Speziale 1993). To prevent an exaggerated wall modification, an alternative to the conventional wall-proximity function in Equation 10 is now considered.

A first approach would be to replace the damping function f with $f(1 - A)$, where the anisotropy parameter A takes the value 1 in isotropic turbulence and becomes zero in the two-component limit. Now, by means of the weighting function $g = (1 - A/A_{\max})^2$, which ranges from zero to unity in the two-component limit, a blending of the two functions f and $f(1 - A)$ yields

$$\begin{aligned} f^{\mathrm{new}} &= f\cdot g + f(1 - A)(1 - g) \\ &= f[(1 - A) + A(1 - A/A_{\max})^2] \end{aligned} \tag{21}$$

where the multiplicative factor within the square brackets is intended to weaken the wall influence in the central region of turbulent channel flows. Here, $A_{\max}$ denotes the highest value of the anisotropy parameter A attained in the actual flow, $A_{\max} = 1$ being its upper bound reached only in fully isotropic turbulence.

3.3. Algebraic Reynolds stress model

Let us now assume that the nonzero components of the Reynolds stress tensor are practically constant in the central core region of the plane Couette flow. The viscous and turbulent stress diffusion can thus be neglected, and Equation 2 for the second-moments reduces to

$$0 = P_{ij} - \varepsilon_{ij} + \phi_{ij} \tag{22}$$

which automatically implies local equilibrium, i.e., $P = \varepsilon$. Although the extent of the core region is marginal in the low-Reynolds-number direct simulation of Kristoffersen et al. (1993), these assumptions are supported by the DNS data (Andersson et al. 1992, 1993). The originally strongly coupled model equations for the individual stress components can now

be manipulated to give a set of explicit algebraic expressions for the Reynolds stresses:

$$\frac{\overline{u^2}}{k} = \frac{2}{3}(1 + b(2 + aC_2C_2^w)) + abC_1^w\frac{\overline{v^2}}{k} \tag{23}$$

$$\frac{\overline{v^2}}{k} = \frac{2}{3}(1 - b(1 + 2aC_2C_2^w))/(1 + 2abC_1^w) \tag{24}$$

$$\frac{\overline{w^2}}{k} = \frac{2}{3}(1 - b(1 - aC_2C_2^w)) + abC_1^w\frac{\overline{v^2}}{k} \tag{25}$$

$$-\frac{\overline{uv}}{k} = \left(\frac{b\left(1 + \frac{3}{2}C_2C_2^w a\right)}{1 + \frac{3}{2}abC_1^w}\cdot\frac{\overline{v^2}}{k}\right)^{1/2} \tag{26}$$

where the new parameters

$$a = f/(1 - C_2) \tag{27}$$

$$b = (1 - C_2)/C_1 \tag{28}$$

have been introduced to simplify the notation. In accordance with the philosophy of near-wall modeling, the functions in Equations 14 to 18 are supposed to take constant values in the core region of the Couette flow.

3.4. Numerical approach

In unidirectional flow problems, like fully developed Poiseuille and Couette flows, the governing set of model equations consists of a single equation for the mean flow, four equations for the nonzero Reynolds-stress components, and the dissipation-rate equation. This set of ordinary differential equations can be solved numerically to practically any degree of accuracy. However, in a preliminary computational study, Andersson et al. (1993) were unable to obtain fully converged solutions with the standard Launder and Shima closure for turbulent Couette flow. Irrespective of the initial field adopted, the turbulence eventually died away.

In the course of the present study, a new numerical solver for unidirectional flow problems has been constructed, in which the numerical stability and computational efficiency have been significantly improved. Spatial derivatives are replaced by second-order accurate central-difference approximations, in which the locations of the shear stress $\overline{uv}$ are staggered with respect to the nodes for the other dependent variables. The resulting difference equations are solved semi-implicitly by a pseudo-time-marching scheme until a converged steady-state solution is reached. A nonuniform distribution of grid points across the flow was used to meet the grid-density requirements suggested by So et al. (1991). Typically, 100 grid points were needed to assure grid independency, and some of the calculations were rerun with 100 percent more points without any discernible effect. For Re above 20,000, the computations were made with 200 points.

4. Asymptotic analysis for high Re

The Reynolds-averaged streamwise momentum equation, Equation 1, can readily be integrated once to give a constant shear stress distribution

$$\tau = \mu\frac{dU}{dy} - \rho\overline{uv} = \rho u_\tau^2 \tag{29}$$

across the flow. Here, the partition among the viscous and turbulent contributions varies substantially across the flow. In the core region, the contribution of the turbulent shear stress $-\rho\overline{uv}$ is substantially greater than that of the viscous shear stress $\mu dU/dy$, and, moreover, the viscous contribution tends to zero in the high-Reynolds-number limit.

For sufficiently high Reynolds numbers, it can therefore be anticipated that $-\rho\overline{uv} \approx \rho u_\tau^2$ in the central core region, and it is furthermore conjectured that $\overline{v^2}$ and k remain constant throughout the core in which local equilibrium conditions $P = \varepsilon$ prevail. Based on these simplifying assumptions, the dissipation rate equation (Equation 12) can be written as

$$0 = \frac{d}{dy}\left[\frac{1}{\varepsilon}\frac{d\varepsilon}{dy}\right] - B^2\varepsilon^2 = 0 \tag{30}$$

where

$$B^2 = \frac{C_{\varepsilon 2} - C_{\varepsilon 1}}{C_\varepsilon}\cdot\frac{1}{k^2\overline{v^2}} \tag{31}$$

becomes a positive constant in the region where $k^2\overline{v^2}$ is uniform. Equation 30 can therefore be integrated analytically to give

$$\varepsilon = \varepsilon_0/\cos(\varepsilon_0 By) \tag{32}$$

where ε_0 denotes the dissipation rate at the centerline. Now, by equating ε to $P = -\overline{uv}\,dU/dy \approx u_\tau^2\,dU/dy$, the explicit formula

$$U = \ln\left[\tan\left(\frac{1}{2}\varepsilon_0 By + \frac{\pi}{4}\right)\right]/\mathrm{Bu}_\tau^2 + \frac{1}{2}U_w \tag{33}$$

can readily be deduced for the variation of the mean velocity in the core region. Here, ε_0 can be obtained from the slope of the mean velocity profile at $y = 0$, i.e., $\varepsilon_0 = u_\tau^2 \cdot dU/dy|_{y=0}$. By adopting the eddy-viscosity concept, Henry and Reynolds (1984) derived an analogous equation for $U(y)$ in the core region.

5. Results and discussion

The Launder and Shima model with the new wall-proximity function defined in Equation 21 has been used to compute plane turbulent Couette flow at Re = 2,600, which matches the Reynolds number adopted in the recent direct numerical simulation of Kristoffersen et al. (1993). Comparisons of the model calculations with DNS data are given in Figure 2. The variation of the mean velocity U across the flow is well reproduced by the model, except in the near-wall region from $0.1\,h$ to $0.3\,h$ away from the walls (see Figure 2a). The overprediction of the mean velocity gradient in this region is more clearly seen in the distribution of the viscous shear stress in Figure 2b, in which the turbulent shear stress $-\rho\overline{uv}$ is correspondingly underestimated. The partition among viscous and turbulent shear is otherwise in close agreement with the DNS data. The profiles of the normal stresses compare reasonably well with the numerical simulations (see Figure 2c). Unlike the plane Poiseuille flow, only the streamwise normal stress exhibits a maximum in the near-wall region. The actual peak level is somewhat underestimated by the model, but this appeared to be a common feature of the eight near-wall closures examined by So et al. (1991). The departure of $\overline{u_iu_j}$ from isotropy in the channel center is faithfully reproduced by the present model, which is closer to the DNS data than the prediction by Sund (1993) (see Table 2). It is moreover noteworthy that computations with the new wall-proximity function and the modified set of model constants suggested by Shima (1993a, 1993b) further improved the results.

It is interesting to recall that the only distinction between Sund's model and the present approach is that Sund (1993)

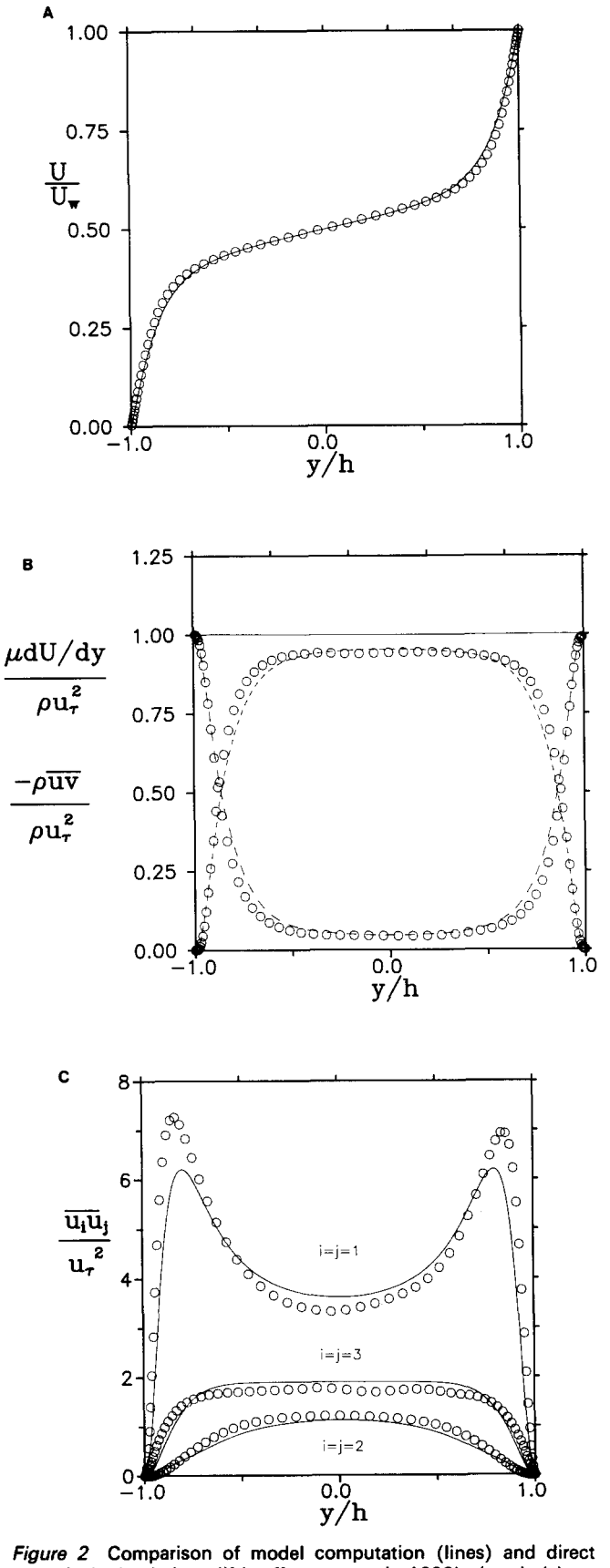

Figure 2 Comparison of model computation (lines) and direct numerical simulation (Kristoffersen et al. 1993) (symbols) at Re = 2,600. (a) Distribution of mean velocity; (b) total (—), turbulent (- - -), and viscous (— —) shear stress; and (c) normal stress components

Table 2 Centerline characteristics for Re = 2,600

	u_τ/U_w	$\overline{u^2}/k$	$\overline{v^2}/k$	$-\overline{uv}/k$	k/u_τ^2
Sund	0.030	1.13	0.30	—	3.46
Present	0.030	1.09	0.34	0.29	3.33
Present[a]	0.032	1.07	0.36	0.29	3.31
DNS	0.032	1.06	0.38	0.30	3.22

[a] With a modified set of model constants due to Shima (1993a, 1993b)

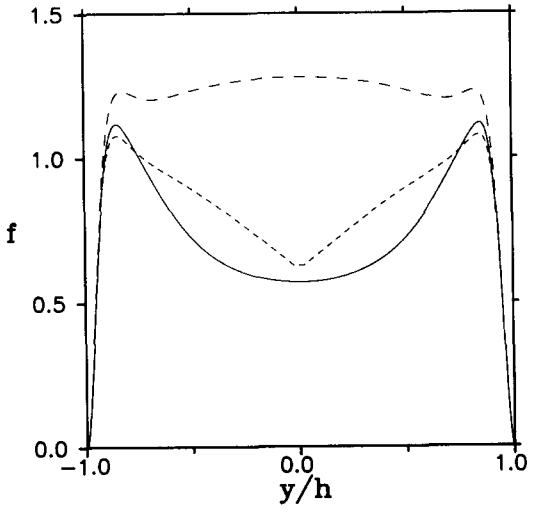

Figure 3 Variation of the wall-proximity function across the Couette channel for Re = 2,600. —, Present approach; - - - -, Sund (1993); — — —, conventional function defined in Equations 10 and 11, deduced from the computed results in Figure 2

used the conventional wall-proximity function f in Equation 10, but with the effective wall-distance d accounting for only one wall at a time. This physically unappealing function exhibits a kink at the midplane, as shown in Figure 3, while the present proposal assures a smooth variation across the flow. In both cases, however, f attains an appreciable level even in the center. Contrary to the arguments of Schneider (1989), this observation demonstrates that inclusion of a wall-correction model is essential to assure a reasonable partition of energy among the normal stresses. This is also in keeping with the conclusion reached by Obi et al. (1989), namely, that model predictions are strongly influenced by the adopted wall-reflection model.

In a preceding study of the same flow by Andersson et al. (1993), the standard Launder and Shima closure, as described in section 3.1, failed to converge. It was believed that the more robust numerical approach described in section 3.4 could remedy this unforeseen failure. However, even if the solution presented in Figure 2 was adopted as the initial field, the turbulence died slowly away as the solution was advanced forward in pseudo-time. The same behavior occurred at Re = 26,000, and we are therefore inclined to conclude that the Launder and Shima model, in its original version (Launder and Shima 1989), is unsuitable for turbulent Couette flow at low and moderate Reynolds numbers.

With the converged solution in Figure 2 available, the original wall-proximity function defined in Equations 10 and 11 can be deduced. The resulting variation of f across the flow

in Figure 3 exhibits a plateau over the region $-0.85\,h < y < +0.85\,h$, with a maximum value above 1.2 in the center. This unreasonable high level of f exaggerates the effect of the wall-reflection model $\phi^{w}_{ij,1} + \phi^{w}_{ij,2}$, which redistributes energy from the normal direction to $\overline{u^2}$ and $\overline{w^2}$. The excess drainage of energy out of $\overline{v^2}$ reduces the magnitude of the shear stress production $P_{12} = -\overline{v^2}\,dU/dy$, thereby damping $-\overline{uv}$ and, ultimately, the overall turbulence level.

The replacement of the original wall-proximity function with the new proposal in Equation 21 was sufficient to make the computations converge to the solution in Figure 2, which compares favorably with the DNS data. To examine whether the introduction of f^{new} deteriorates the model performance in other flow situations, the benchmark problem adopted by So et al. (1991) was considered. The plane Poiseuille flow at $Re_\tau = u_\tau h/\nu = 180$ was computed and compared with the direct numerical simulation of Kim et al. (1987) in Figure 4. The deviation between the computations with the original and the new f-function is negligible in the near-wall region as expected, whereas the new wall-proximity function has a favorable effect throughout the region $-0.9\,h < y < +0.9\,h$.

Due to computer limitations, DNS is feasible only at low Reynolds number, while the turbulence model should be applicable at any Re. Couette flow computations have therefore been carried out also at Re = 4,762 and Re = 35,000. Comparisons with recent laboratory measurements by Aydin and Leutheusser (1987, 1991) and Tillmark and Alfredsson (1993) in Figure 5 show the same tendencies as in Figure 2, namely, that the peak level of the streamwise turbulence intensity is somewhat underestimated (Figure 5b) as is the mean velocity gradient dU/dy around the peak (Figure 5a). However, the streamwise intensity is slightly underpredicted in the core region in comparison with the experimental results in Figure 5b, while the predicted level of $\overline{u^2}$ exceeded the DNS data in Figure 2c.

At the significantly higher Reynolds number Re = 35,000, shown in Figure 6, the predicted mean velocity profile (Figure 6a) is consistent with the experimental data (Robertson and Johnson 1970; El Telbany and Reynolds 1980; Reichardt 1959), while the scatter in the experimentally obtained intensities in Figure 6b does not allow any firm conclusions to be drawn.

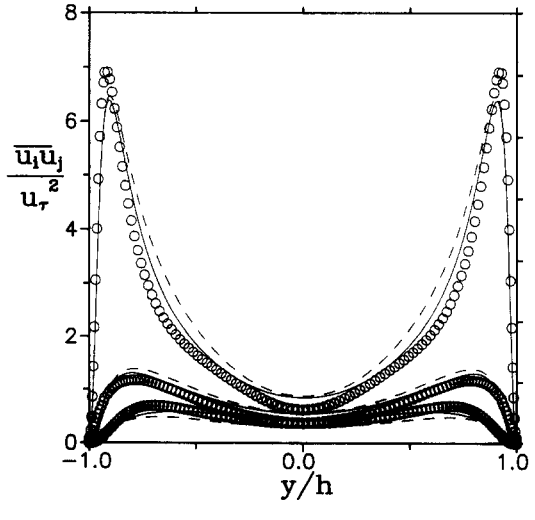

Figure 4 Comparison of model computations and direct numerical simulation of plane Poiseuille flow at $Re_\tau = 180$. —, Present computation; ---, original Launder and Shima closure; ○, DNS (Kim et al. 1987)

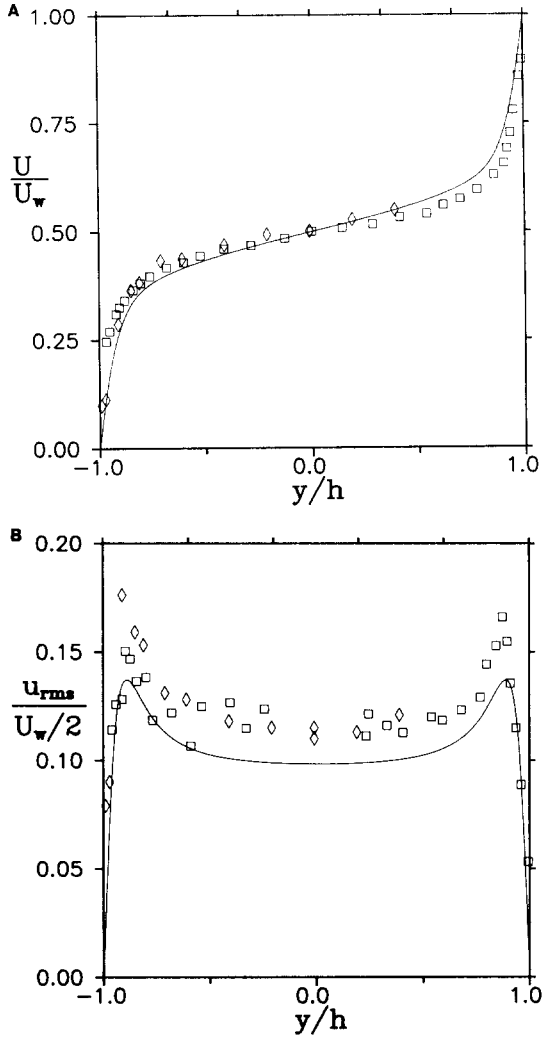

Figure 5 Comparison of model computation and experimental data. —, Present computation, Re = 4,762; □, Aydin and Leutheusser (1991), Re = 4,762; ◇, Tillmark and Alfredsson (1993), Re = 4,600. (a) Distribution of mean velocity; (b) streamwise turbulence intensity

A notable distinction between the computations presented in Figures 2 and 6 is that the characteristic wall layers occupied nearly 50 percent of the channel at Re = 2,600, while the core extends over more than 90 percent of the cross section at Re = 35,000. The outstanding features of the core region are therefore more easily revealed at higher Re. The profiles of the predicted turbulence intensities in Figure 6b show that the turbulent kinetic energy is uniform throughout the core. At this Re, it can also be observed that the diffusion terms vanish and leave a balance between stress production, pressure-strain redistribution, and dissipation, as hypothesized in Equation 22. The production rate P of the kinetic energy k is thus balanced by its dissipation rate ε, both varying across the channel. It is also interesting to observe that the low-Re expressions in Equations 14 to 18 attain constant values in the core region, and these values moreover appear to be practically independent of the Reynolds number for Re > 20,000. These high-Re asymptotes have been used to compute the Reynolds stress components from the algebraic model equations (Equations 23 to 26) for f-values ranging from 0 to 1 (see Figure 7). In accordance with the intention of the wall-reflection model, the

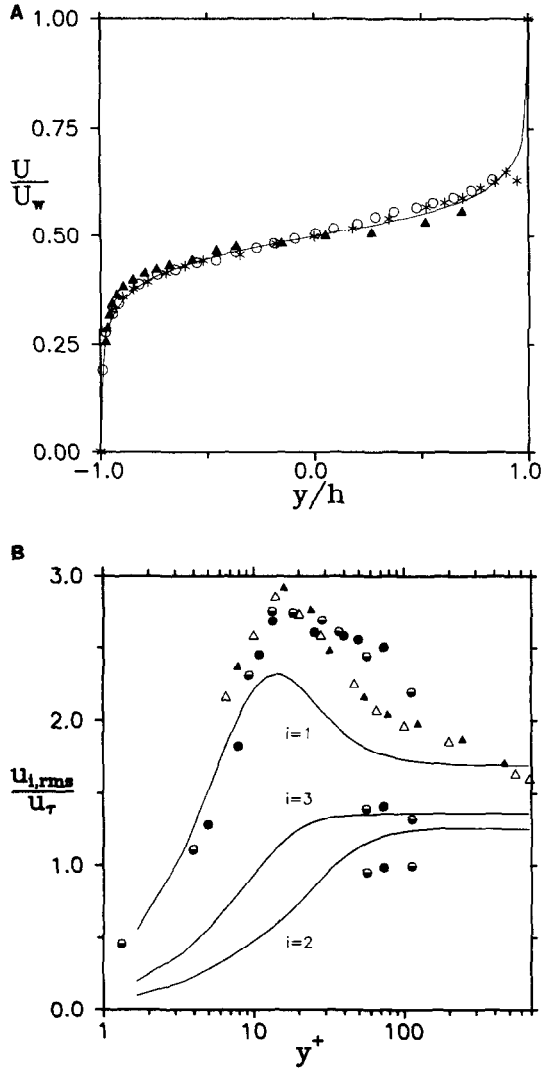

Figure 6 Comparison of model computation and experimental data. —, Present computation, Re = 35,000; *, Reichardt (1959), Re = 34,000; △, Robertson and Johnson (1970), Re = 28,200; ▲, Robertson and Johnson (1970), Re = 33,000; ○, El Telbany and Reynolds (1980), Re = 28,500; ◒, El Telbany and Reynolds (1981), Re = 28,500; ●, El Telbany and Reynolds (1982), Re = 37,920. (*a*) Distribution of mean velocity; (*b*) turbulence intensities

anisotropy increases with f, i.e., as the wall-reflections become more influential. Midplane values arising from the full second-moment closure predictions have also been included in the figure. The substantial difference between the circles and the lines indicates that at least some of the assumptions underlying the ASM model are not fulfilled at Re = 2,600. On the other hand, the excellent agreement at Re = 35,000 demonstrates that all the simplifications are justified at higher Re. The explicit algebraic model equations (Equations 23 to 26) can therefore be used as a diagnostic tool to elucidate the influence of the wall-proximity function on the stress anisotropy.

The numerical solutions for high-Re Couette flow confirmed the validity of the assumptions used in section 4. It is therefore interesting to observe from the close-up in Figure 8a that the analytical solution (Equation 33) closely approximates the model predictions for $-0.25\,h < y < +0.25\,h$ even for the

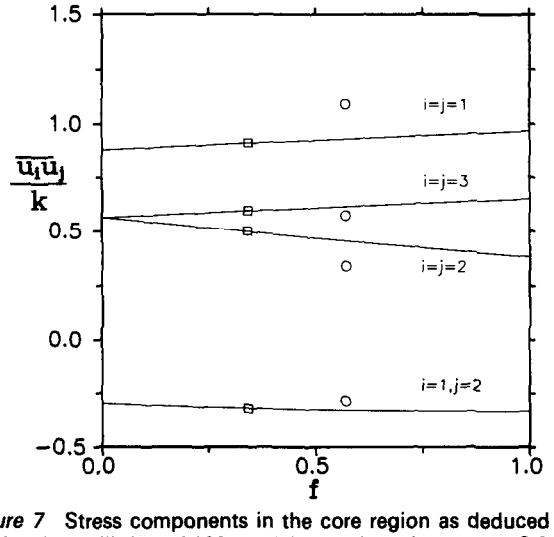

Figure 7 Stress components in the core region as deduced from the local-equilibrium ASM model equations in section 3.3 with the high-Re asymptotes $C_1 = 2.33$, $C_2 = 0.63$, $C_1^w = 0.11$, *and* $C_2^w = 0.40$. The symbols denote full second-moment closure predictions. ○, Re = 2,600; □, Re = 35,000

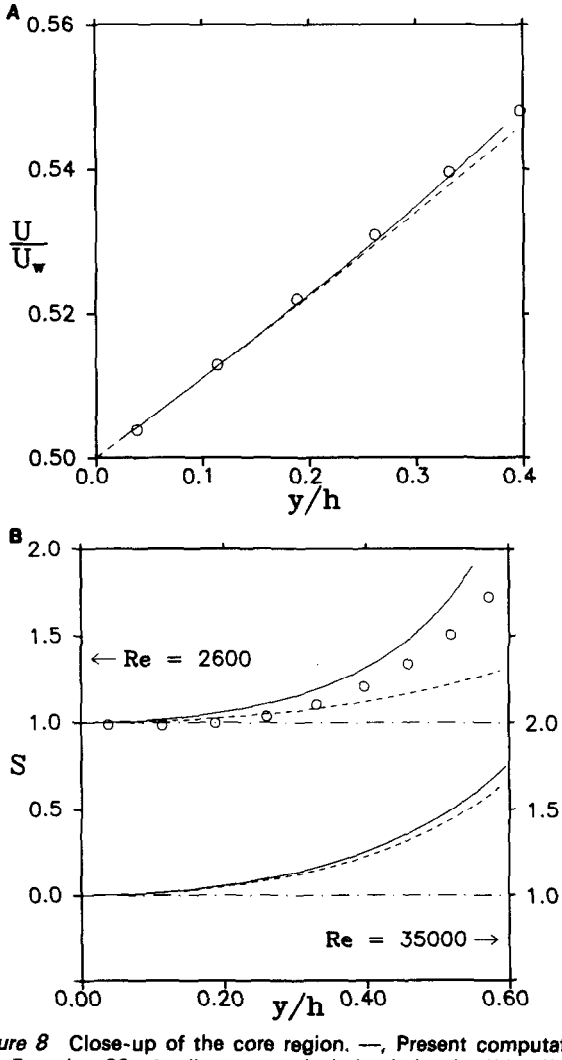

Figure 8 Close-up of the core region. —, Present computation; - - -, Equation 33; ○, direct numerical simulation by Kristoffersen et al. (1993); —·—, reference line dU/dy = constant. (a) Distribution of mean velocity U for Re = 2,600; (b) distribution of mean shear rate dU/dy ($S = (dU/dy)/(dU/dy)_{y=0}$)

lowest Re = 2,600, whereas Figure 8b shows that Equation 33 accurately approximates the full transport model over at least 60 percent of the channel at Re = 35,000. However, the variation of dU/dy in the central portion of the Couette flow, as suggested by Equation 33 and reproduced by the model, is intuitively in conflict with the assumption of quasi-homogeneous shear flow. This observation signals a deficiency of the modeled ε-equation (Equation 12), which can only be remedied if the otherwise unacceptable relationship $C_{\varepsilon 1} = C_{\varepsilon 2}$ is adopted. Contrary to the model predictions, however, the DNS data for Re = 2,600 exhibit a strictly linear variation of U in the center region (see also the variation of dU/dy in Figure 8b), thereby supporting the existence of von Kármán's hypothesized homologous or quasi-homogeneous core in plane Couette flow.

Finally, the predicted variation of the skin-friction coefficient $C_f \equiv 2(\tau_w/\rho)/(U_w/2)^2 = 8(u_\tau/U_w)^2$ with Re is compared with measured values and DNS data in Figure 9, whereas corresponding center-line characteristics are listed in Table 3. The solid lines in Figure 9 represent the semiempirical correlation formula

$$C_f = \alpha[\log(\mathrm{Re}/2)]^{-2} \tag{34}$$

derived by Robertson and Johnson (1970). The two lines correspond to values of the dimensionless constant α equal to 0.072 and 0.066, as suggested by Robertson and Johnson (1970) and El Telbany and Reynolds (1982), respectively. It is encouraging to observe that the model predictions broadly follow the trend of the data. It is particularly noteworthy that the turbulence vanishes at Re = 1,000 and that the solution conforms with the exact correlation

$$C_f = 4 \cdot \mathrm{Re}^{-1} \tag{35}$$

for laminar flow. In spite of the great scatter in the reported values of the transitional Reynolds number, above which fully developed turbulence can be sustained, the most recent investigations by Tillmark and Alfredsson (1992) suggest Re_{tr} to be 720 ± 20, whereas earlier studies reported Re_{tr} in the range of 560 to 1,500.

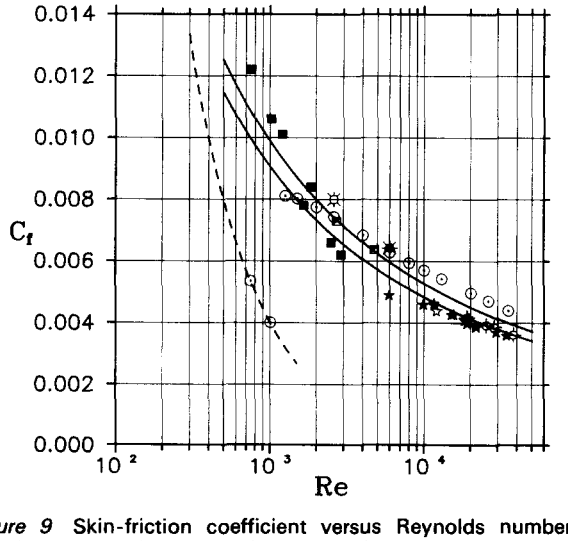

Figure 9 Skin-friction coefficient versus Reynolds number.—, Correlation formula in Equation 34, with α equal to 0.072 and 0.066; - - -, correlation in Equation 35 for laminar flow; ⊙, present computations; ☼, DNS (Kristoffersen et al. 1993); ✳, DNS (Lee and Kim 1991); ★, Reichardt (1959) (taken from Chue and McDonald 1970); ☆, Chue and McDonald (1970); ■, Leutheusser and Chu (1971); ◩, Aydin and Leutheusser (1991); ☼, El Telbany and Reynolds (1982)

Table 3 Centerline characteristics for different Re

Re	u_τ/U_w	$\overline{u^2}/k$	$\overline{v^2}/k$	$-\overline{uv}/k$	k/u_τ^2
1,500	0.032	1.40	0.13	0.18	4.83
2,000	0.031	1.22	0.24	0.25	3.78
2,600	0.030	1.09	0.34	0.29	3.33
4,762	0.029	0.94	0.47	0.31	3.11
10,000	0.027	0.91	0.50	0.32	3.10
20,000	0.025	0.91	0.50	0.32	3.11
35,000	0.023	0.91	0.50	0.32	3.15

6. Concluding remarks

The paper has focused on second-moment modeling of the conceptually simple Couette flow between two parallel planes in relative motion. The wall-proximity function f in the wall-reflection term, which is added to the model for the pressure-strain process, has been identified as the source of our inability to make the well-established Launder and Shima model converge. More specifically, an exaggerated energy transfer from $\overline{v^2}$ to $\overline{u^2}$ resulted from an overestimated f in the core region. Since the introduction of a wall correction term is a common feature of many second-moment closures, the same tendency is likely to be found also with other turbulence closures for this particular flow. With the inclusion of a new wall-proximity function, however, a more realistic partition of turbulence energy among the normal stresses is assured, and the computations are in better accordance with DNS data and the most reliable experimental results than any of the previous attempts to calculate this flow.

Closer examination of the computed results reveals that the modeled Couette flow exhibits a local-equilibrium core region the relative extension of which increases with Re. The substantial anisotropy of the Reynolds stress tensor observed in the direct simulation at Re = 2,600 is satisfactorily reproduced by the model. At higher Re, the explicit algebraic expressions for the individual Reynolds stresses accurately reproduced the stress anisotropy obtained from the full Reynolds stress transport model, thereby forming a practical diagnostic tool freed from numerical inaccuracies and the actual choice of model equation for the energy dissipation rate.

Acknowledgments

The authors are grateful to Knut H. Bech and Reidar Kristoffersen for many helpful discussions.

References

Abid, R. and Speziale, C. G. 1993. Predicting equilibrium states with Reynolds stress closures in channel flow and homogeneous shear flow. *Phys. Fluids A*, **5**, 1776–1782

Andersson, H. I., Bech, K. H., and Kristoffersen, R. 1992. On diffusion of turbulent energy in plane Couette flow. *Proc. R. Soc. Lond. A*, **438**, 477–484

Andersson, H. I., Bech, K. H., and Kristoffersen, R. 1993. Reynolds-stress budgets in plane Couette flow: Direct simulation and second-moment modelling. In *Engineering Turbulence Modelling and Experiments*, vol. 2. Elsevier, Amsterdam, 293–302

Aydin, E. M. and Leutheusser, H. J. 1987. Experimental investigation of turbulent plane Couette flow. *ASME Forum on Turbulent Flows, FED* **51**, 51–54

Aydin, E. M. and Leutheusser, H. J. 1991. Plane-Couette flow between smooth and rough walls. *Exp. Fluids*, **11**, 302–312

Chue, S. H. and McDonald, A. T. 1970. Application of a new effective viscosity model to turbulent plane Couette flow. *AIAA J.*, **8**, 2076–2078

El Telbany, M. M. M. and Reynolds, A. J. 1980. Velocity distributions in plane turbulent channel flows. *J. Fluid Mech.*, **100**, 1–29

El Telbany, M. M. M. and Reynolds, A. J. 1981. Turbulence in plane channel flow. *J. Fluid Mech.*, **111**, 283–318

El Telbany, M. M. M. and Reynolds, A. J. 1982. The structure of turbulent plane Couette flow. *ASME J. Fluids Eng.*, **104**, 367–372

Gibson, M. M. 1988. Analysis of turbulent Couette flow with a Reynolds stress model. MED Report FS/88/54, Imperial College, London

Gibson, M. M. and Launder, B. E. 1978. Ground effects on pressure fluctuations in the atmospheric boundary layer. *J. Fluid Mech.*, **86**, 491–511

Henry, F. S. and Reynolds, A. J. 1984. Analytical solution of two gradient-diffusion models applied to turbulent Couette flow. *ASME J. Fluids Eng.*, **106**, 211–216

Kim, J., Moin, P., and Moser, R. 1987. Turbulence statistics in fully developed channel flow at low Reynolds number. *J. Fluid Mech.*, **177**, 133–166

Kristoffersen, R., Bech. K. H., and Andersson, H. I. 1993. Numerical study of turbulent plane Couette flow at low Reynolds number. *Appl. Sci. Res.*, **51**, 337–343

Launder, B. E. and Shima, N. 1989. Second-moment closure for the near-wall sublayer: development and application. *AIAA J.*, **27**, 1319–1325

Lee, M. J. and Kim, J. 1991. The structure of turbulence in a simulated plane Couette flow. *Proc. Eighth Symp. Turbulent Shear Flows*, Munich, 5.3.1–5.3.6

Leutheusser, H. J. and Chu, V. H. 1971. Experiments on plane Couette flow. *ASCE J. Hydraul. Div.*, **97**, 1269–1284

Monnier, J. C. and Stanislas, M. 1989. Critical examination of various turbulence models applied to different one dimensional internal flows. *Proceedings of the Sixth International Conference on Numerical Methods in Laminar and Turbulent Flow, Part 1.* Pineridge Press, Swansea, 297–306

Nisizima, S. and Yoshizawa, A. 1987. Turbulent channel and Couette flows using an anisotropic k–ε model. *AIAA. J.*, **25**, 414–420

Obi, S., Perić, M., and Scheuerer, G. 1989. Computation of plane Couette flow by a Reynolds-stress closure model. Technical Note, LSTM Erlangen, Erlangen, Germany

Reichardt, H. 1959. Gesetzmässigkeiten der geradlinigen turbulenten Couetteströmung. Mitteilung Nr. 22, Max-Planck-Institut für Strömungsforschung, Göttingen

Robertson, J. M. and Johnson, H. F. 1970. Turbulence structure in plane Couette flow. *ASCE J. Eng. Mech. Div.*, **96**, 1171–1182

Schneider, W. 1989. On Reynolds stress transport in turbulent Couette flow. *Zeitschrift für Flugwissenschaften und Weltraumforschung*, **13**, 315–319

Shima, N. 1993a. Prediction of turbulent boundary layers with a second-moment closure: Part I—Effects of periodic pressure gradient, wall transpiration, and free-stream turbulence. *ASME J. Fluids Eng.*, **115**, 56–63

Shima, N. 1993b. Prediction of turbulent boundary layers with a second-moment closure: Part II—Effects of streamline curvature and spanwise rotation. *ASME J. Fluids Eng.*, **115**, 64–69

So, R. M. C., Lai, Y. G., Zhang, H. S., and Hwang, B. C. 1991. Second-order near-wall turbulence closures: a review. *AIAA J.*, **29**, 1819–1835

Sund, H. 1993. Validation of a second-moment closure to low Reynolds number plane Couette flow. *Proceedings of the Eighth International Conference on Numerical Methods in Laminar and Turbulent Flow, Part 1.* Pineridge Press, Swansea, 241–248

Tillmark, N. and Alfredsson, P. H. 1992. Experiments on transition in plane Couette flow. *J. Fluid Mech.*, **235**, 89–102

Tillmark, N. and Alfredsson, P. H. 1993. Turbulence in plane Couette flow. *Appl. Sci. Res.*, **51**, 237–241

von Kármán, T. 1937. The fundamentals of the statistical theory of turbulence. *J. Aeronaut. Sci.*, **4**, 131–138

Zhang, H. S., So, R. M. C., and Zhu, M. L. 1993. A near-wall second-order turbulence model for wall-bounded flows. *Proc. Ninth Symp. Turbulent Shear Flows*, Kyoto, 8.2.1–8.2.6